Narrow-Waisted Gaussian Beams for Aperture-Generated Scattering From Planar Conducting Surfaces With Complex Coatings Described by Higher Order Impedance Boundary Conditions

Vincenzo Galdi, *Member, IEEE*, Leopold B. Felsen, *Life Fellow, IEEE*, and Innocenzo M. Pinto, *Member, IEEE*

***Abstract*—In this paper, we use higher order impedance boundary conditions (HOIBCs) for studying high frequency asymptotic two-dimensional (2-D) scattering of *truncated aperture-generated* electromagnetic fields from planar conducting surfaces coated by multiple layers of homogeneous bi-anisotropic media. The reflected field syntheses are carried out via asymptotic reduction of *rigorous* plane-wave spectral integrals, which are subsequently discretized and transformed to the spatial domain through use of a Gabor-based narrow-waisted (NW) Gaussian beam (GB) algorithm. In this discretized algorithm, the GB propagators are approximated by previously explored standard and modified (uniform) complex-source-point paraxial asymptotic techniques. Example applications are restricted to zeroth and second order IBCs for single- and multilayer complex coatings, with emphasis on the adaptation of the NW-GBs to the HOIBC launch conditions in the presence of localizing (e.g., focused and/or abruptly truncated) illumination. The results confirm that the previously established utility of the NW-GB algorithm with respect to accuracy and computational feasibility continues to hold for this fairly general combination of environmental complexity and strongly inhomogeneous (localizing) illumination.**

***Index Terms*—Bianisotropic layered media, Gaussian beam asymptotics, higher order impedance boundary conditions.**

I. Introduction

ANALYSIS of electromagnetic (EM) time-harmonic scattering from metallic objects coated by thin layers of composite materials is an important problem which arises in many applications ranging from design of microwave absorbers to analysis of radar signatures. During the last decade, this problem has attracted renewed interest related to advances in materials technology which have allowed the actual manufacturing of novel artificial media such as uniaxial chiral [1] and negative-refraction [2] materials. Anticipated capabilities for realizing classes of exotic "complex media" with *bianisotropic* propagation and scattering properties [3] will endow the designer with new perspectives on circuit components and devices [4]–[6]. While most theoretical aspects pertaining to the electrodynamics of such materials are already well understood (see, e.g., [7] and the references therein for a comprehensive review), their utilization as composite *smart* coatings for metallic objects is still a largely open issue whose investigation requires effective simulation tools. In this connection, use of *rigorous* analytical (spectral) techniques is restricted to canonical coordinate-separable (i.e., planar, circular cylindrical, spherical) geometries (see, e.g., [8], [9]), whereas numerical techniques [10], [11], though more generally applicable, usually require rather cumbersome and computationally demanding implementations which do not contribute much physical insight. The use of approximate impedance boundary conditions (IBCs), formalized by differential equations which relate the tangential (or normal) electric and magnetic field components at the interface between the coated object and free space, provides an attractive framework for both analytical and numerical implementation in these complex wave scattering scenarios. The coefficients in such differential equations depend on the local properties of the coating as well as on the frequency; solutions are usually obtained by solving suitable canonical problems or via Taylor series expansion of the fields.

Derivations and applications of IBCs for wave propagation and scattering in acoustics, electromagnetics, hydrodynamics, etc., are available in the technical literature (see [12]–[33] for a sparse sampling). Starting from the simplest and well-known Leontovich-type IBCs [12], which do not contain field derivatives and can be applied only to electrically thin and/or considerably dense/lossy coatings [15], more sophisticated IBCs with a wider range of applicability have been developed via the inclusion of appropriate higher order field derivatives [13], [14], [16]–[21]. Such IBCs are usually referred to as *generalized* IBCs or *higher- order* IBCs (HOIBCs). Up to the second order, they have been applied successfully to a variety of EM scattering problems involving homogeneous and inhomogeneous dielectric (multi-)layers [13]–[27], [29], dielectric-filled grooves [19], [22], bianisotropic coatings [28], [31], [32], nonlinear media [30], etc.

Manuscript received April 14, 2003; revised July 2, 2003. The work of L. B. Felsen was supported in part by the US-Israel Binational Science Foundation, Jerusalem, Israel, under Grant 9900448 and in part by Polytechnic University, Brooklyn, NY 11201 USA.

V. Galdi and I. M. Pinto are with the Waves Group, Department of Engineering, University of Sannio, I-82100 Benevento, Italy (e-mail: vgaldi@unisannio.it; pinto@sa.infn.it).

L. B. Felsen is with the Department of Aerospace and Mechanical Engineering and the Department of Electrical and Computer Engineering, Boston University, Boston, MA 02215 USA and also with the Polytechnic University, Brooklyn, NY 11201 USA (e-mail: lfelsen@bu.edu).

Digital Object Identifier 10.1109/TAP.2004.827486

Expanding upon the conventional canonical excitations, the scattering of *truncated large phased-aperture-generated* incident high-frequency (HF) fields by thinly coated HOIBC surfaces would appear to be of interest for more "realistic" applications. To address such problems efficiently, we explore in the present paper the utilization of Gabor-based narrow-waisted (NW) quasiray Gaussian beam algorithms, which have emerged in the last decade as attractive alternatives to traditional ray methods for wave propagation and scattering in complex environments [34]–[41] by overcoming failures near caustics and other transition regions, while preserving the attractive computational features of ray field tracking in the presence of electrically large computational domains.

To the best of our knowledge, HOIBC-parameterized *phased* (including *focused*)-*aperture-excited* HF scattering has not been investigated elsewhere in the technical literature. For our example configuration, we have chosen a planar geometry for which a rigorous reference solution is available, thereby allowing for systematic validation and calibration. Solutions for this canonical problem category, naturally addressed in the *spectral domain*, constitute the building blocks for more general applications involving *gently curved* surfaces and/or *slowly varying* coating parameters. Anticipating such extensions, our field syntheses are eventually recast in the *spatial domain* so as to facilitate their *local* (adiabatic) application. The coatings to be explored are composed of multiple layers of materials with general linear bi-anisotropic constitutive relationships, which have recently received attention as potential candidates for reduced-reflection surface treatments [6]. For such coatings, the HOIBC approach proposed by Hoppe and Rahmat-Samii [22] and implemented up to the second order, as well as its subsequent generalizations in [29] and [31], have been found effective and systematic and will therefore be pursued in our investigation.

The remainder of the paper is organized as follows. In Section II, the HF scattering problem is formulated and the notation utilized throughout the paper is introduced. In Section III, the field reflected by the coating is derived, evolving from the rigorous spectral (plane-wave) synthesis to the HF approximate Gabor-based beam syntheses. In this connection, previously used standard and new guided/leaky-mode-induced (uniform) complex-source-point (CSP) paraxial asymptotic techniques are utilized for effective closed-form approximations of the IBC-matched discretized beam propagators. It is shown that conventional continuous Kirchhoff-type integral formulations can be obtained from such CSP beam syntheses in the limit of vanishing complex displacement (i.e., vanishing NW beam waist). Section IV contains numerical results, with accuracy assessments and discussion of computational issues. Conclusions are summarized in Section V. The reader is referred to [22], [31], [35], [38], [41], for theoretical and computational details on the HOIBCs and on the NW-GB algorithms (see also the brief Appendixes).

II. Problem Formulation

A. Physical Configuration

The problem geometry is shown in Fig. 1. An aperture-generated incident field illuminates a planar perfectly conducting surface with a planar penetrable (possibly composite) coating of total thickness d_c. The incident field is generated by a large (arbitrarily phased) truncated aperture field distribution of width d, located at $z = z_A$, where the tangential (x, y) field components are specified

$$\mathbf{E}_t^i(x, z_A) = \begin{cases} \mathbf{F}(x), & |x| \le \frac{d}{2}, \\ 0, & |x| > \frac{d}{2}, \end{cases} \tag{1}$$

$$\mathbf{F}(x) = F_x(x)\mathbf{u}_x + F_y(x)\mathbf{u}_y. \tag{2}$$

Here and henceforth, an implicit $\exp(-i\omega t)$ harmonic time dependence is assumed and suppressed. Bold face symbols denote vector quantities, the subscript "$_t$" denotes tangential (i.e., (x, y) plane) fields, and $\mathbf{u}_\alpha$ denotes an α-directed unit vector. The assumed planar multilayer coatings are composed of homogeneous linear materials with general (bianisotropic) constitutive relationships [42],

$$\begin{cases} \mathbf{D} = \epsilon_0(\underline{\underline{\boldsymbol{\epsilon}}}_r \cdot \mathbf{E} + \eta_0 \underline{\underline{\boldsymbol{\xi}}} \cdot \mathbf{H}), \\ \mathbf{B} = \mu_0 \left(\underline{\underline{\boldsymbol{\mu}}}_r \cdot \mathbf{H} + \eta_0^{-1} \underline{\underline{\boldsymbol{\zeta}}} \cdot \mathbf{E} \right) \end{cases} \tag{3}$$

where ϵ_0 and μ_0 are the free-space electric permittivity and magnetic permeability, respectively, $\eta_0 = \sqrt{\mu_0/\epsilon_0}$ is the free-space characteristic impedance, and $\underline{\underline{\boldsymbol{\epsilon}}}_r$, $\underline{\underline{\boldsymbol{\mu}}}_r$, $\underline{\underline{\boldsymbol{\xi}}}$, $\underline{\underline{\boldsymbol{\zeta}}}$ are dimensionless dyadics which, in the assumed Cartesian coordinate system, are represented as 3×3 matrices; a double underline denotes dyadic operators. For possible extensions including, e.g., corrugated surfaces and longitudinally inhomogeneous (i.e., in the direction normal to the boundary) dielectric layers, see [22], [29], [31]. The interface between the coating and free space is assumed to be located at $z = 0$, and the coating is assumed to be electrically *thin*. As in [31], we consider rotationally symmetric coatings, whose constitutive properties are invariant under an arbitrary rotation around the z-axis. Under these symmetry assumptions, which arise in many situations of practical interest (e.g., chiral materials, normally biased ferrites, normally uniaxial crystals), and with the excitation in (1), the problem is reduced to a two-dimensional (2-D) form, with all fields and quantities independent of y. Note that, despite the above 2-D reduction, the problem is *not scalar* in general, since the coating may exhibit polarization-rotating properties [22]. Our interest lies in computing the reflected field in the halfspace $z > 0$.

B. High-Order Impedance Boundary Conditions

We deal with a general class of HOIBCs at the interface separating the coating and free space $(z = 0)$, which are defined as follows:

$$\begin{cases} \displaystyle\sum_{\nu=0}^{N} i^{-\nu} \left[c_{1,\nu} \frac{\partial^\nu}{\partial x^\nu} E_{x0}(x) + c_{2,\nu} \frac{\partial^\nu}{\partial x^\nu} E_{y0}(x) \right] \\ \quad \approx \displaystyle\sum_{\nu=0}^{N} i^{-\nu} \left[c_{5,\nu} \frac{\partial^\nu}{\partial x^\nu} H_{x0}(x) + c_{6,\nu} \frac{\partial^\nu}{\partial x^\nu} H_{y0}(x) \right], \\ \displaystyle\sum_{\nu=0}^{N} i^{-\nu} \left[c_{3,\nu} \frac{\partial^\nu}{\partial x^\nu} E_{x0}(x) + c_{4,\nu} \frac{\partial^\nu}{\partial x^\nu} E_{y0}(x) \right] \\ \quad \approx \displaystyle\sum_{\nu=0}^{N} i^{-\nu} \left[c_{7,\nu} \frac{\partial^\nu}{\partial x^\nu} H_{x0}(x) + c_{8,\nu} \frac{\partial^\nu}{\partial x^\nu} H_{y0}(x) \right]. \end{cases} \tag{4}$$

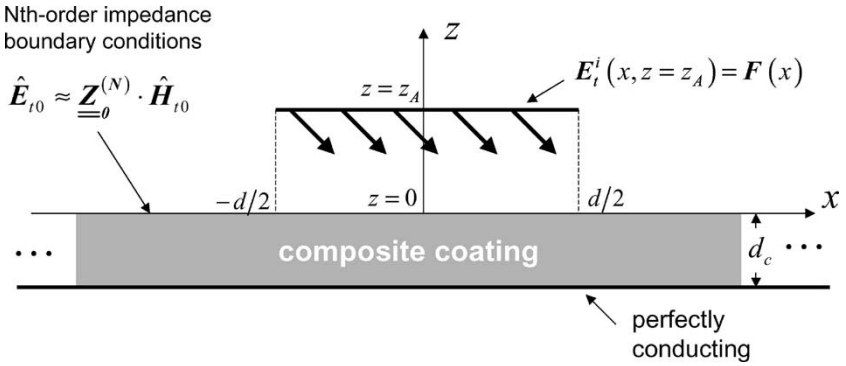

Fig. 1. Problem schematic: a large truncated aperture field distribution $\mathbf{F}(x)$ of width d at $z = z_A$ radiates in the presence of a perfectly conducting planar surface with a thin penetrable coating of total thickness d_c and top surface at $z = 0$. The coating is composed of multiple layers of bi-anisotropic materials, and is described via the Nth-order impedance boundary conditions in (4) or their spectral counterpart in (7). The reflected field is observed in the halfspace $z > 0$.

In (4), the approximate "$\approx$" symbol refers to the truncation at order N of the rigorous $N \to \infty$ sum in the exact IBC; the subscript "$_0$" denotes field quantities evaluated at the interface $z = 0$, and $c_{\mu,\nu}$, $\mu = 1, \ldots, 8$ are constant coefficients depending on the frequency and on geometrical and constitutive properties of the coating. The highest order N of the field derivatives involved in (4) will be referred to as the "order" of the IBCs (in our applications in Section IV, we shall use $N \leq 2$, as in [22]). The assumed rotational invariance introduces some constraints in these coefficients. In particular, $c_{\mu,\nu} = 0$ for ν odd (i.e., only even-order derivatives appear); for relations among the nonzero coefficients, see [22, Appendix B], and Appendix A for the case of zeroth- and second-order IBCs.

The wavenumber spectral domain will be accessed via the spatial Fourier transform pair

$$\hat{F}(k_x) = \int_{-\infty}^{\infty} F(x) \exp(-ik_x x) dx,$$
$$F(x) = \frac{1}{2\pi} \int_{-\infty}^{\infty} \hat{F}(k_x) \exp(ik_x x) dk_x \tag{5}$$

with k_x denoting the x-domain wavenumber, and the caret $\hat{}$ denoting plane-wave spectra. Accordingly, in the wavenumber spectral domain, the algebrization of the spatial derivatives $(\partial^\nu / \partial x^\nu \to (ik_x)^\nu)$ reduces the HOIBCs into compact matrix form

$$\underline{\underline{\mathbf{P}}}_E^{(N)} \cdot \hat{\mathbf{E}}_{t0} \approx \underline{\underline{\mathbf{P}}}_H^{(N)} \cdot \hat{\mathbf{H}}_{t0} \tag{6}$$

or equivalently

$$\hat{\mathbf{E}}_{t0} \approx \underline{\mathbf{Z}}_0^{(N)} \cdot \hat{\mathbf{H}}_{t0},$$
$$\underline{\mathbf{Z}}_0^{(N)} \equiv \begin{bmatrix} Z_{0xx}^{(N)} & Z_{0xy}^{(N)} \\ Z_{0yx}^{(N)} & Z_{0yy}^{(N)} \end{bmatrix} = \left[\underline{\underline{\mathbf{P}}}_E^{(N)}\right]^{-1} \cdot \underline{\underline{\mathbf{P}}}_H^{(N)} \tag{7}$$

where $^{-1}$ denotes the inverse operator and

$$\underline{\underline{\mathbf{P}}}_E^{(N)} \equiv \begin{bmatrix} P_1^{(N)}(k_x) & P_2^{(N)}(k_x) \\ P_3^{(N)}(k_x) & P_4^{(N)}(k_x) \end{bmatrix},$$
$$\underline{\underline{\mathbf{P}}}_H^{(N)} \equiv \begin{bmatrix} P_5^{(N)}(k_x) & P_6^{(N)}(k_x) \\ P_7^{(N)}(k_x) & P_8^{(N)}(k_x) \end{bmatrix} \tag{8}$$

with $P_\mu^{(N)}(k_x)$, $\mu = 1, \ldots, 8$, denoting Nth degree polynomials in k_x

$$P_\mu^{(N)}(k_x) = \sum_{\nu=0}^{N} c_{\mu,\nu} k_x^\nu, \quad \mu = 1, \ldots, 8. \tag{9}$$

It follows from (7)–(9) that the approximated components of the dyadic spectral impedance in (7) are *finite-order rational* functions of the spectral wavenumber k_x. Recalling that for the present geometry one can derive *exact* spectral domain IBCs [31, Section 2.1] in terms of *meromorphic* functions (i.e., with an infinite number of pole singularities), the approximate HOIBCs in (4) can be viewed as a *spectral truncation* (in terms of finite-order rational functions) of the exact $(N \to \infty)$ IBCs; their validity is consequently restricted to a limited spectral range. Within the context of the subsequently imposed $N \leq 2$ constraint, we shall explore to what extent this limited spectral range of validity is capable of accommodating the spatially wide (spectrally confined) aperture field distributions of interest here. For our intended applications, we shall follow the approach of Hoppe and Rahmat-Samii [22] (and its generalization in [31]) to obtain the HOIBCs (see also Section IV and Appendix B).

Since the analytic manipulations that follow are formally independent of the order of the IBCs in (4), the superscript $^{(N)}$ will be dropped from here on for simplicity of notation.

III. Reflected Field Synthesis

A. Solution in the Spectral Domain

For the assumed geometry, the reflected field due to the illuminating field in (1), and with the spectral domain HOIBCs in (7), can be synthesized rigorously in the wavenumber spectral domain. The high-frequency (HF) Gabor-based NW-GB syntheses in Section III-B evolve from the rigorous spectral domain formulation. Using (7) together with simple plane-wave concepts, the reflected and incident field plane-wave spectra at the interface $z = 0$, denoted by $\hat{\mathbf{E}}_0^r$ and $\hat{\mathbf{E}}_0^i$, respectively, can be related via a dyadic (matrix) reflection coefficient

$$\hat{\mathbf{E}}_0^r(k_x) = \begin{bmatrix} \hat{E}_{0,\|}^r(k_x) \\ \hat{E}_{0,\perp}^r(k_x) \end{bmatrix} = \underline{\underline{\mathbf{\Gamma}}}(k_x) \cdot \hat{\mathbf{E}}_0^i(k_x)$$
$$= \begin{bmatrix} \Gamma_{\|,\|}(k_x) & \Gamma_{\|,\perp}(k_x) \\ \Gamma_{\perp,\|}(k_x) & \Gamma_{\perp,\perp}(k_x) \end{bmatrix} \cdot \begin{bmatrix} \hat{E}_{0,\|}^i(k_x) \\ \hat{E}_{0,\perp}^i(k_x) \end{bmatrix}. \tag{10}$$

The fields in (10) have been decomposed into the two standard parallel ($\|$) and perpendicular ($\perp$) polarization states, with respect to the incidence plane (see Fig. 2). The dyadic reflection coefficient is given by

$$\underline{\underline{\mathbf{\Gamma}}}(k_x) = -\left[\underline{\underline{\mathbf{M}}}_E(k_x) + \underline{\underline{\mathbf{Z}}}_0(k_x)\cdot\underline{\underline{\mathbf{M}}}_H(k_x)\right]^{-1} \cdot\left[\underline{\underline{\mathbf{M}}}_E(k_x) - \underline{\underline{\mathbf{Z}}}_0(k_x)\cdot\underline{\underline{\mathbf{M}}}_H(k_x)\right] \quad (11)$$

where (see [22, App. D] for details)

$$\underline{\underline{\mathbf{M}}}_E(k_x) = \begin{bmatrix} \frac{k_z}{k_0} & 0 \\ 0 & 1 \end{bmatrix}, \quad \underline{\underline{\mathbf{M}}}_H(k_x) = \eta_0^{-1}\begin{bmatrix} 0 & \frac{k_z}{k_0} \\ -1 & 0 \end{bmatrix}, \quad k_z = \sqrt{k_0^2 - k_x^2}, \quad \mathrm{Re}(k_z) \geq 0. \quad (12)$$

In (12), $k_0 = \omega\sqrt{\epsilon_0\mu_0} = 2\pi/\lambda_0$ is the free-space wavenumber, with λ_0 denoting the free-space wavelength, and k_z is the longitudinal wavenumber. The expressions in (10)–(12) are slightly different from those in [22] due to the different time dependence and axis orientation here. The reflected field in the halfspace $z > 0$ is readily obtained by propagating the spectrum in (10) via plane-wave superposition [43]. Using simple plane-wave algebra, the result can be expressed conveniently in Cartesian coordinates as

$$\mathbf{E}^r(x,z) \equiv \begin{bmatrix} E_x^r \\ E_y^r \\ E_z^r \end{bmatrix} = \frac{1}{2\pi}\int_{-\infty}^{\infty} \underline{\underline{\mathbf{R}}}(k_x)\cdot\hat{\mathbf{E}}_{t0}^i(k_x) \times \exp\left[i(k_x x + k_z z)\right] dk_x, \quad (13)$$

where $\underline{\underline{\mathbf{R}}}$ is a Cartesian dyadic reflection coefficient,

$$\underline{\underline{\mathbf{R}}}(k_x) = \begin{bmatrix} \left(\frac{k_z}{k_0}\right)^2 \Gamma_{\|,\|}(k_x) & \frac{k_z}{k_0}\Gamma_{\|,\perp}(k_x) \\ \frac{k_z}{k_0}\Gamma_{\perp,\|}(k_x) & \Gamma_{\perp,\perp}(k_x) \\ -\frac{k_x k_z}{k_0^2}\Gamma_{\|,\|}(k_x) & -\frac{k_x}{k_0}\Gamma_{\|,\perp}(k_x) \end{bmatrix} \quad (14)$$

and $\hat{\mathbf{E}}_{t0}^i$ denotes the Cartesian tangential (x,y) incident field plane-wave spectrum at the interface $z = 0$, which is tied to the spectrum of the aperture field distribution in (2) via

$$\hat{\mathbf{E}}_{t0}^i(k_x) = \hat{\mathbf{F}}(k_x)\exp(ik_z z_A). \quad (15)$$

Numerical brute-force integration of (13) will be used in Section IV to obtain a reference solution for calibrating and validating the NW-GB syntheses discussed next.

B. HF Asymptotics: Gabor-Based Beam Synthesis

Starting from (13), a conventional spatial-domain Kirchhoff-type integral formulation of the reflected HF field can be obtained by substituting the Fourier integral pertaining to $\hat{\mathbf{E}}_{t0}^i(k_x)$ and performing the spectral integration asymptotically. In this synthesis, the reflected field is launched from an equivalent aperture plane by the illumination-generated equivalent sources. In what follows, we shall derive an alternative synthesis based on the analytic explicit Gabor-discretized NW-GB algorithm. This formulation is more flexible and efficient, and reduces in the continuous limit to a Kirchhoff-type integral formulation. Recalling the efficient treatment of linearly phased

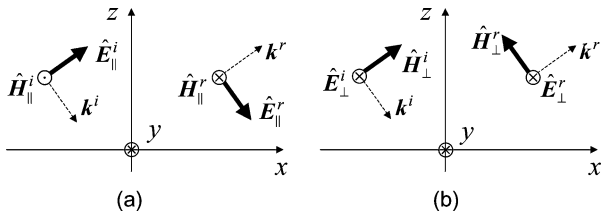

Fig. 2. Incident and reflected field decomposition. (a): Parallel ($\|$) polarization; (b): perpendicular ($\perp$) polarization. $\mathbf{k}^i$ and $\mathbf{k}^r$ denote the incident and reflected wavevectors, respectively.

aperture field distributions in Gabor-based GB algorithms (see [38], [41]), we first rewrite the aperture field distribution in (2) as

$$\mathbf{F}(x) = \mathbf{G}(x)\exp(ik_0 x\sin\theta_A), \quad (16)$$

where the linear phasing term has been separated out. In (16), θ_A is a real tilt angle, and $\mathbf{G}(x)$ is a complex (possibly nonlinearly phased) vector function. Generalizing the approach in [38], [41] to the vector case, we then expand $\mathbf{G}(x)$ into a Gabor series [44]

$$\mathbf{G}(x) = \sum_{m,n=-\infty}^{\infty} \mathbf{A}_{mn} w(x - x_m)\exp(in\beta_x x) \quad (17)$$

where $x_m = mL_x$, and $w(x)$ represents the normalized Gaussian window (initial beam profile)

$$w(x) = \left(\frac{\sqrt{2}}{L_x}\right)^{\frac{1}{2}} \exp\left[-\pi\left(\frac{x}{L_x}\right)^2\right], \quad \hat{w}(k_x) = (\sqrt{2}L_x)^{\frac{1}{2}} \exp\left[-\pi\left(\frac{k_x}{\beta_x}\right)^2\right]. \quad (18)$$

This formal complete representation places the beam basis functions on a discretized (x, k_x) phase-space lattice, on which each lattice point gives rise to a GB whose spatial and spectral (beam tilt) shifts are tagged by the indexes m and n, respectively. Spatial and spectral periods are related by the configuration-spectrum tradeoff $L_x\beta_x = 2\pi$ [44]. The vector expansion coefficients $\mathbf{A}_{mn}$ in (17) can be computed in principle by introducing an auxiliary *bi-orthogonal* function [44], but our subsequent use of narrow-waisted beams allows a simpler and more efficient approximate estimation [38], [41]. By substituting the Gabor expansion of $\mathbf{G}(x)$ in (17) into the expression for $\mathbf{F}(x)$ in (16), one obtains via Fourier transform [see (15)] the following expansion for the tangential incident field plane-wave spectrum at the interface $z = 0$,

$$\hat{\mathbf{E}}_{t0}^i(k_x) = \sum_{m,n=-\infty}^{\infty} \mathbf{A}_{mn}\hat{w}(k_x - k_0\sin\theta_A - n\beta_x) \times \exp\left\{-i\left[(k_x - k_0\sin\theta_A)x_m - k_z z_A\right]\right\}. \quad (19)$$

The corresponding Gabor lattice representation of the reflected field follows directly by combining (13) and (19), and can be expressed concisely as

$$\mathbf{E}^r(x,z) = \sum_{m,n=-\infty}^{\infty} \underline{\underline{\mathbf{B}}}_{mn}(x,z)\cdot\mathbf{A}_{mn} \quad (20)$$

where $\underline{\underline{\mathbf{B}}}_{mn}$ are dyadic beam propagators

$$\begin{aligned}\underline{\underline{\mathbf{B}}}_{mn}(x,z) &= \frac{1}{2\pi}\int_{-\infty}^{\infty}\underline{\underline{\mathbf{R}}}(k_x)\hat{w}(k_x-k_0\sin\theta_A-n\beta_x)\\ &\quad\times\exp\{i\left[k_x(x-x_m)+k_0\sin\theta_A x_m\right.\\ &\quad\left.+k_z(z+z_A)\right]\}\,dk_x\\ &= \frac{(\sqrt{2}L_x)^{\frac{1}{2}}}{2\pi}\int_{-\infty}^{\infty}\underline{\underline{\mathbf{R}}}(k_x)\exp\left[k_0 r_m\psi_{nm}(k_x)\right]dk_x, \quad (21)\end{aligned}$$

with $r_m=\sqrt{(x-x_m)^2+(z+z_A)^2}\geq 0$ and

$$\begin{aligned}\psi_{mn}(k_x) &= (k_0 r_m)^{-1}\{i\left[k_x(x-x_m)+k_0\sin\theta_A x_m\right.\\ &\quad\left.+k_z(z+z_A)\right]-\pi\beta_x^{-2}(k_x-k_0\sin\theta_A-n\beta_x)^2\}. \quad (22)\end{aligned}$$

The dyadic beam propagators in (21) can be viewed as a generalization of the vector beam propagators in [34]. Their tensor nature arises from the assumed *full* polarization of the incident field, whereas the presence of the (dyadic) spectral reflection coefficient $\underline{\underline{\mathbf{R}}}$ accounts for the effect of the coating. The approximate asymptotic reduction of the spectral integral in (21) will be performed via standard and modified CSP paraxial asymptotics.

1) Narrow-Waisted Beams and Regular Reflection Coefficient: Nonuniform Complex-Source-Point Paraxial Asymptotics: As in [38], [41] we use propagation-matched ($n=0$) *narrow-waisted* (NW) beams ($L_x\lesssim\lambda_0\ll d$), which have several attractive features. First, the evaluation of the formally messy Gabor vector amplitude coefficients $\mathbf{A}_{m0}$ in (20) can be carried out effectively by mere *sampling* of the aperture field distribution at the lattice points x_m (for simplicity of notation, the subscript "$_{m0}$" is henceforth replaced by "$_m$")

$$\mathbf{A}_m\approx\left(\frac{L_x}{\sqrt{2}}\right)^{\frac{1}{2}}\mathbf{G}(mL_x),\quad |m|\leq\frac{d}{(2L_x)}. \quad (23)$$

In free space, the wide *spectral* spacing (i.e., large "tilt" intervals) arising from the tight *spatial* packing under NW conditions (due to the Gabor spatial-spectral tradeoff) was found to drive all $n\neq 0$ beams away from the aperture into the evanescent range. These beams, tilted with respect to θ_A, were therefore ignored [38]. In the presence of a penetrable coating, evanescent constituents may interact with the structure so as to couple to possible surface-wave fields, but their contribution is still negligible (exponentially decaying) for observation and aperture distances sufficiently far from the coating. Under these conditions, the NW beam synthesis of the reflected field involves only an aperture-filling finite series of propagating beams

$$\mathbf{E}^r(x,z)\sim\sum_{|m|\leq\frac{d}{(2L_x)}}\underline{\underline{\mathbf{B}}}_m(x,z)\cdot\mathbf{A}_m. \quad (24)$$

In [35], [36] an effective reduction of the NW beam propagator integral in (21) is obtained via saddle-point (SP) methods and CSP paraxial asymptotics applied to the phase function in (22). Here, care should be taken due to the presence of the dyadic spectral reflection coefficient $\underline{\underline{\mathbf{R}}}$ in (21), which may contain *pole singularities* close to the SP (poles have *not* been encountered in our previous NW-GB investigations [34]–[41]). For *regular* reflection coefficients (i.e., with pole singularities sufficiently far from the SP), generalization of the standard nonuniform SP CSP asymptotics in [35] is rather straightforward. One obtains the following expression for the dyadic NW beam propagator

$$\begin{aligned}\underline{\underline{\mathbf{B}}}_m(x,z)\sim\tilde{\underline{\underline{\mathbf{B}}}}_m(x,z) &= -i2^{\frac{5}{4}}\underline{\underline{\mathbf{R}}}(\tilde{k}_{xs})\,(z-\tilde{z}')\\ &\quad\times\left(\frac{k_0L_x}{8\pi\tilde{R}_m^3}\right)^{\frac{1}{2}}\exp\left[i\tilde{\phi}_m(x,z)\right] \quad (25)\end{aligned}$$

where

$$\tilde{\phi}_m(x,z)=k_0(\tilde{R}_m+x_m\sin\theta_A+ib)+\frac{\pi}{4} \quad (26)$$

and $\tilde{R}_m$ represents the complex distance

$$\tilde{R}_m=\sqrt{(x-\tilde{x}'_m)^2+(z-\tilde{z}')^2},\quad \mathrm{Re}(\tilde{R}_m)\geq 0 \quad (27)$$

between the observer at $\mathbf{r}\equiv(x,z)$ and the CSP located on the image plane $z=-z_A$

$$\tilde{\mathbf{r}}'_m\equiv(\tilde{x}'_m,\tilde{z}')=(x_m+ib\sin\theta_A,-z_A+ib\cos\theta_A). \quad (28)$$

Here and henceforth, a tilde ($\tilde{}$) superscript on a quantity denotes its extension into a complex coordinate space. The CSP displacement parameter (Fresnel length) b in (26) and (28) is related to the beam lattice period L_x and the tilt angle θ_A via $b=(L_x\cos\theta_A)^2/\lambda_0$ [35]. Moreover, in (25), $\tilde{k}_{xs}$ denotes the approximate complex SP

$$\tilde{k}_{xs}\approx k_0\frac{(x-\tilde{x}'_m)}{\tilde{R}_m} \quad (29)$$

obtained via analytic continuation (to $\tilde{\mathbf{r}}'_m$ in (28) of the real SP derived from (22) with $n=0$ and $L_x=0$. The CSP asymptotic result in (25) is valid in the paraxial far-zone of each beam, $|\tilde{R}_m|\gg b$. Apart from their tensor structure, the corresponding beam propagators are formally similar to the CSP NW-GB propagators in [35] but they are no longer paraxially Gaussian, due to the modulation introduced by the spectral reflection coefficient. These wave objects will be referred to as dyadic narrow-waisted "standard modulated Gaussian beams" (NW-SMGBs). Note that in the limit of zero spacing ($L_x=0$), the beam synthesis in (24) reduces to a conventional Kirchhoff-type continuous superposition of *real-source* ($b=0$) contributions (cylindrical waves).

2) Narrow-Waisted Beams and Singular Reflection Coefficient: Uniform Complex-Source-Point Paraxial Asymptotics: If the spectral reflection coefficient has pole singularities close to the SP, the nonuniform approximation in (25) breaks down, and must be replaced by modified uniform asymptotics [45, Sec. 4.4]. Here, by addition and subtraction, it is convenient to split the dyadic spectral reflection coefficient as follows:

$$\underline{\underline{\mathbf{R}}}(k_x)=\underline{\underline{\mathbf{R}}}^{(reg)}(k_x)+\underline{\underline{\mathbf{R}}}^{(sing)}(k_x), \quad (30)$$

where the superscript $^{(reg)}$ denotes the *regular* (i.e., singularity-free) part, whereas the superscript $^{(sing)}$ denotes the *singular* part. The (standard) regular part can be handled as in Section III-B1. In the spectral range of interest (i.e., where the incident field is significantly nonzero), the singular part can be approximated "reasonably well" by a finite number of dominant poles (those closest to the SP). These poles should

not be confused with the poles of the spectral impedances discussed in Section II-B. For a generic element of the $\underline{\underline{\mathbf{R}}}$ dyadic (3×2 matrix) in (14), tagged by the indices pq ($p = 1$, 2, 3, $q = 1$, 2), one should therefore derive a finite-order approximate partial-fraction (pole-residue) expansion

$$\left[\underline{\underline{\mathbf{R}}}^{(sing)}(k_x)\right]_{pq} \approx \sum_{l=1}^{M_{pq}} \frac{\alpha_{pql}}{k_x - \kappa_{pql}}, \quad p = 1,2,3, \quad q = 1,2 \tag{31}$$

with κ_{pql} and α_{pql} denoting the poles and corresponding residues, respectively. Estimating such poles and residues, as well as the order M_{pq}, constitutes a typical *model-based parameter estimation* problem [46], which can be addressed in several ways. Here, we used a simple scheme based on type-II Padé (rational) approximants [47, Sec. 1.2.2]. In this scheme (see Section IV-A for details), a point-matching procedure is employed to determine a rational approximation of $[\underline{\underline{\mathbf{R}}}^{(sing)}(k_x)]_{pq}$, which is then recast in the pole-residue form of (31). For implementation of the asymptotics corresponding to (31), we employed the Van der Waerden modified saddle-point procedure for integrands with poles [45, Section 4.4], which yields a *uniform* approximation. The reflected field is thus synthesized as follows:

$$\mathbf{E}^r(x,z) \sim \sum_{|m| \le \frac{d}{(2L_x)}} \left[\tilde{\underline{\underline{\mathbf{B}}}}_m^{(\mathrm{reg})}(x,z) + \tilde{\underline{\underline{\mathbf{D}}}}_m(x,z)\right] \cdot \mathbf{A}_m \tag{32}$$

where $\tilde{\underline{\underline{\mathbf{B}}}}_m^{(\mathrm{reg})}$ is the dyadic NW-MGB propagator in (25) with $\underline{\underline{\mathbf{R}}}$ replaced by $\underline{\underline{\mathbf{R}}}^{(\mathrm{reg})}$, whereas $\tilde{\underline{\underline{\mathbf{D}}}}_m$ is a dyadic beam propagator whose generic pq element has the following closed-form expression, valid for $k_0 r_m \gg 1$:

$$\begin{aligned}
&\left[\tilde{\underline{\underline{\mathbf{D}}}}_m(x,z)\right]_{pq} \\
&\quad = 2^{\frac{-3}{4}} \sqrt{\frac{L_x}{\pi}} \sum_{l=1}^{M_{pq}} \kappa_{pql} \\
&\qquad \times \Big\{ \pm 2i \exp\left(-k_0 r_m \tilde{\rho}_{pql}^2\right) \\
&\qquad\quad \times \left[Q\left(\mp i \tilde{\rho}_{pql} \sqrt{k_0 r_m}\right) - \sqrt{\pi} U\left(\mp \mathrm{Im}(\kappa_{pql})\right) \right] \\
&\qquad\quad + \frac{1}{\tilde{\rho}_{pql} \sqrt{k_0 r_m}} \Big\}, \\
&\qquad \mathrm{Im}(\tilde{\rho}_{pql}) \lessgtr 0, \quad p = 1,2,3, \quad q = 1,2.
\end{aligned} \tag{33}$$

In (33), $U(\cdot)$ is the Heaviside's step function, and $Q(\cdot)$ is the error function complement [48, Section 7]

$$Q(\xi) = \int_{\xi}^{\infty} \exp(-\zeta^2) d\zeta, \quad Q(\xi) + Q(-\xi) = \sqrt{\pi}. \tag{34}$$

Moreover,

$$\tilde{\rho}_{pql} = \mathrm{sign}\left\{ \mathrm{Re}\left[\frac{\tilde{\chi}_{pql} \exp\left(-\frac{i\pi}{4}\right)}{\kappa_{pql} - \tilde{k}_{xs}} \right] \right\} \tilde{\chi}_{pql}, \tag{35}$$

$$\tilde{\chi}_{pql} = \sqrt{\psi_m(\tilde{k}_{xs}) - \psi_m(\kappa_{pql})}, \quad \mathrm{Re}(\tilde{\chi}_{pql}) \ge 0 \tag{36}$$

with ψ_m corresponding to ψ_{m0} in (22). The asymptotic approximation in (33) is valid *uniformly* as $\tilde{k}_{xs} \to \kappa_{pql}$, although a slight deterioration in accuracy is to be expected when using the approximate saddle-point $\tilde{k}_{xs}$ in (29). The wave objects $\tilde{\underline{\underline{\mathbf{D}}}}_m$ in (32) will be referred to as dyadic NW "uniform modulated Gaussian beams" (NW-UMGBs). The use of CSP-analytically continued *uniform* beam propagators has also been explored by Cheung and Jull [49] in a different context involving edge diffraction problems. Note also that the uniform beam synthesis in (32) reduces to a uniform Kirchhoff-type integral formulation in the limit as L_x (and hence b) tends to zero.

IV. Examples of Application

A. Implementation Details and Simulation Parameters

An extensive series of numerical experiments has been carried out in order to validate and calibrate the beam syntheses developed in Sections III-B1 and III-B2. As mentioned before, we used IBCs of order $N \le 2$. Our reference solution is obtained from brute-force numerical quadrature (five-point Gaussian [50], 20 points per spectral period) of the exact plane-wave spectral representation for the reflected field in (13). This solution incorporates the *exact* spectral IBCs (and thus the exact dyadic reflection coefficients), computed via the systematic procedure in [31, Sec. 2.1]. Moreover, in order to facilitate the numerical integration, the spatial distribution $\mathbf{F}(x)$ of the aperture field in all simulation examples below has been chosen so as to render the plane-wave spectrum in (15) computable analytically in closed form.

Concerning the choice of beam syntheses and HOIBCs, we have selected three interesting combinations: *i*) UMGBs (cf. (32)) and second-order IBCs, *ii*) SMGBs (cf. (24)) and second-order IBCs, and *iii*) SMGBs and zeroth-order IBCs. In all examples, zeroth- and second-order IBCs were derived using the systematic spectral domain procedure in [22], [31] (see also Appendix B). For second-order IBCs, exact and approximated IBCs were matched at three spectral directions $k_x = 0$, $k_0/2$ and k_0, spanning the entire visible range. Zeroth-order (Leontovich-type) IBCs were determined by matching the exact and approximated IBCs at normal incidence ($k_x = 0$) only.

For UMGBs, the pole-residue approximation in (31) was obtained via type-II Padé (rational) approximants [47, Sec. 1.2.2]. Note that, as a consequence of the assumed symmetry in the problem, $\underline{\underline{\mathbf{Z}}}_0^{(N)}$ in (7) and $\underline{\underline{\mathbf{\Gamma}}}$ in (11) are even functions of k_x. It follows from (14) that the elements in $\underline{\underline{\mathbf{R}}}$ consist of even functions of k_x, possibly multiplied by k_x. Accordingly, it is expedient to approximate the even parts in terms of rational functions in the variable k_x^2, so as to reduce the number of unknown parameters. From this approximation, determined via point matching [47, Section 1.2.2], the decomposition as in (30) and (31) follows via straightforward analytic manipulations, recalling the simple identity

$$\frac{k_x}{k_x - \kappa} = 1 + \frac{\kappa}{k_x - \kappa}. \tag{37}$$

Concerning the choice of M_{pq}, although no simple rule of thumb can be provided, general guidelines can be found in [46], [47, Sec. 1.2.2]. We merely note that increasing M_{pq}, though introducing a number of spurious poles, tends to improve the localization of the *dominant* poles and thus the overall accuracy; accordingly, we simply increased the number of poles progressively until a satisfactory fit was achieved. As

a general remark, rational approximants in the variable k_x^2 with third-degree numerator and denominator (i.e., $M_{pq} = 6$), were found to yield uniformly accurate results for all examples presented below. In this connection, the matching points were chosen as evenly spaced in the visible range. The complex-argument error function complement in (33) was computed using the series approximations in [48, Section 7], [51].

In all simulations, the number of beams $N_b = d/L_x$ retained in the expansions was arrived at following the pragmatic stability criterion in [35], based on the insensitivity of the result with respect to different combinations ("scramblings") of the beam/lattice configuration.

B. Numerical Results

The materials and parameter configurations in the examples below were chosen to challenge the NW-GB algorithm with nontrivial complex scattering scenarios and exaggerated cross-polarization effects. No effort was made at this preliminary stage to relate the synthetic model to practical feasibility.

1) Example 1: Single-Layer Chiral Coating and Focused Illumination: As a first example of application, we consider a single-layer chiral coating, described by the following constitutive tensors [42]

$$\underline{\underline{\boldsymbol{\epsilon}}}_r = \epsilon_r \underline{\underline{\mathbf{I}}}, \quad \underline{\underline{\boldsymbol{\mu}}}_r = \mu_r \underline{\underline{\mathbf{I}}},$$
$$\underline{\underline{\boldsymbol{\xi}}} = i(\epsilon_0\mu_0)^{-\frac{1}{2}}\gamma_c \underline{\underline{\mathbf{I}}}, \quad \underline{\underline{\boldsymbol{\zeta}}} = -i\mu_r\eta_0\gamma_c \underline{\underline{\mathbf{I}}} \tag{38}$$

where $\underline{\underline{\mathbf{I}}}$ denotes the unit dyadic, and γ_c is the chiral admittance. Exact and approximated IBCs (in the form as in (4)) have been derived by Hoppe and Rahmat-Samii [22, Sec. 3.3]. Apart from the importance of artificially synthesized chiral materials for practical microwave and antenna applications [1], these materials furnish a convenient meaningful challenging test configuration which exhibits nonconventional reflection characteristics with cross-polarization effects [42], modeled in terms of relatively few constitutive parameters. This renders extensive parametric calibrations computationally feasible.

The excitation in this example is a perpendicularly polarized Gaussian-tapered tilted focusing aperture field distribution as in (16) with

$$\mathbf{G}(x) = \exp\left(-\alpha\frac{x^2}{d^2} + ik_0\beta x^2\right)\mathbf{u}_y, \quad \beta < 0 \tag{39}$$

with the conventional focal distance defined as $L_f = -1/(2\beta)$. The aperture is assumed to be rather large ($d = 20\lambda_0$), with $z_A = 5\lambda_0$. As a consequence of the chirality-induced cross-polarization effects, the reflected field has all three Cartesian components (via the nonzero cross-coupling term $\Gamma_{||,\perp}$ in (14)).

The exact and approximated spectral impedance components in (7) are displayed in Fig. 3 over the entire visible (propagating) range, based on the parameter configuration specified in the figure caption. For this example, as a consequence of power conservation and reciprocity [22, App. A], the impedance terms are purely imaginary; reciprocity also dictates that $Z_{0yy} = -Z_{0xx}$ [22, App. A]. It is observed from Fig. 3 that the spectral impedances exhibit pole singularities at $k_x \approx \pm 0.25k_0$ (corresponding to spectral directions of about $\pm 15^\circ$ from the z-axis). Because of their rational structure, even the second-order IBCs

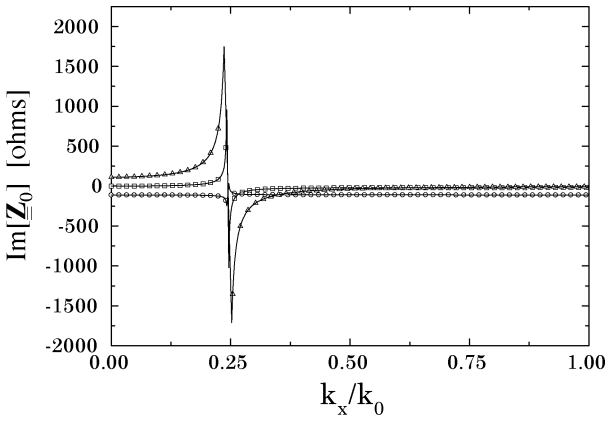

Fig. 3. Example 1: spectral impedances. Chiral coating as in (38), with $\epsilon_r = 4$, $\mu_r = 2$, $\gamma_c = 0.05$ ohm^{-1}, $d_c = 0.1\lambda_0$. Exact and second-order spectral reactance terms in (7) in the visible range; real parts are zero due to power conservation (lossless layer) and reciprocity. Due to symmetry, only positive spatial frequencies are displayed. Squares, circles and triangles: exact Z_{0xx}, Z_{0xy} and Z_{0yx}, respectively. Solid curves: 2nd-order approximations (matching points at $k_x = 0, k_0/2, k_0$). Note that $Z_{0yy} = -Z_{0xx}$ due to reciprocity. Also, note the pole singularity at $k_x \approx \pm 0.25k_0$. Zeroth-order (Leontovich-type) approximations (not displayed) are constant and matched to the exact impedances at $k_x = 0$.

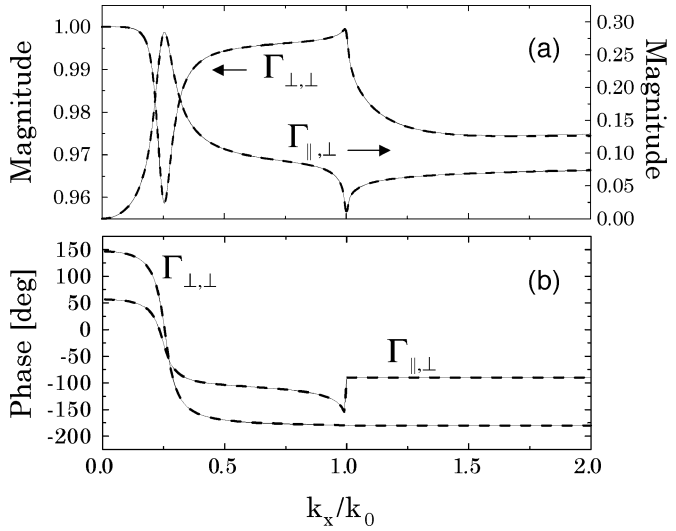

Fig. 4. Example 1: spectral reflection coefficients. Chiral coating with parameters as in Fig. 3. Spectral reflection coefficients in (11) pertaining to perpendicular-polarization incidence: $\Gamma_{\perp,\perp}$ (copolar), $\Gamma_{||,\perp}$ (cross-polar). Due to symmetry, only positive spatial frequencies are displayed. (a): Magnitude; note the different scales for copolar (left) and cross-polar (right). (b): Phase. —— Exact; - - - Computed via 2nd-order IBCs (matching points at $k_x = 0$, $k_0/2, k_0$). The peaks/valleys around $k_x \approx \pm 0.25k_0$ arise from complex (leaky wave) poles at $k_x \approx \pm(0.247 + i0.036)$. For 0th-order (Leontovich-type) IBCs (not displayed), $\Gamma_{||,\perp}$ is uniformly zero, whereas $\Gamma_{\perp,\perp}$ has unit magnitude in the visible range and exhibits a pole singularity in the invisible range at $k_x \approx \pm 3.49k_0$.

are remarkably capable of homing in on these singularities, and provide uniformly accurate approximations. In this connection, the choice of the three matching points (see Appendix B) was found to be not particularly critical. As an aside, zeroth-order (Leontovich-type) IBC approximations (not displayed) are considerably less accurate, being trivially constant and matched with the exact spectral impedances at $k_x = 0$; at the thereby implied normal incidence, one loses the impedance terms Z_{0xx} and Z_{0yy} which are responsible for cross-polarization. Moreover, in

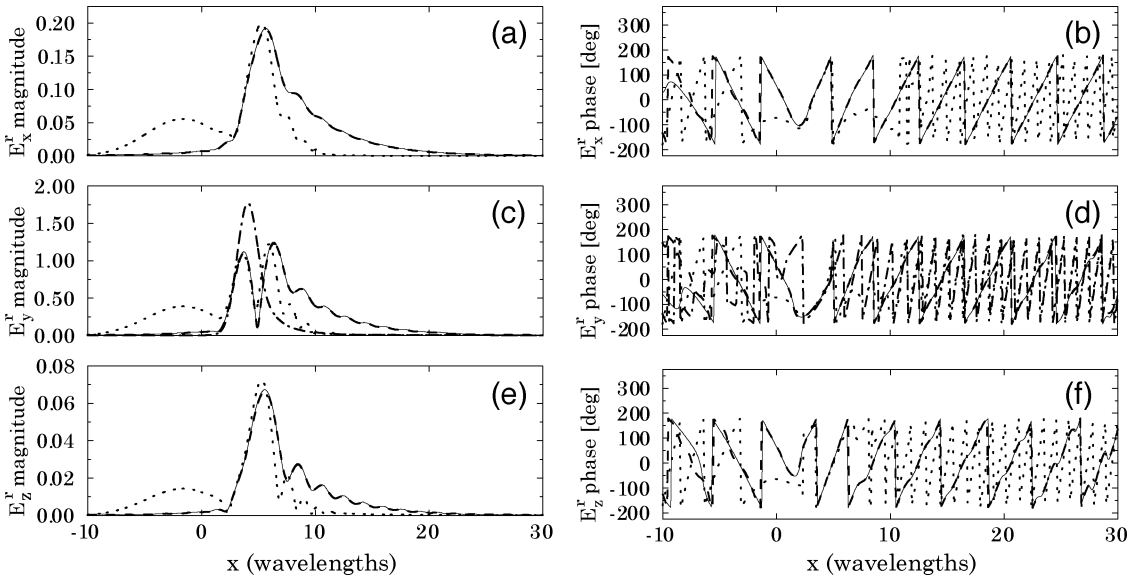

Fig. 5. Example 1: reflected fields. Chiral coating with parameters as in Fig. 3, and y-polarized Gaussian-tapered tilted focusing aperture field distribution as in (16) and (39), with $d = 20\lambda_0$, $z_A = 5\lambda_0$, $\theta_A = 15^0$, $\alpha = 20$, $\beta = -1/(30\lambda_0)$ (i.e., $L_f = 15\lambda_0$). Near-zone reflected fields at $z = 10\lambda_0$. (a), (c), (e): E_x^r, E_y^r, E_z^r magnitude, respectively. (b), (d), (f): E_x^r, E_y^r, E_z^r phase, respectively. —— Reference solution (spectral integration); - - - NW-UMGB synthesis with 2nd-order IBCs ($N_b = d/L_x = 50$ beams) $\cdots\cdots$ NW-SMGB synthesis with 2nd-order IBCs ($N_b = d/L_x = 50$ beams); $-\cdot-\cdot-\cdot-$ NW-SMGB synthesis with zeroth-order IBCs ($N_b = d/L_x = 50$ beams), displayed only in Figs. (c) and (d) (field is zero in all other cases). For UMGBs, the pole-residue approximation (31) was obtained using $M_{pq} = 6\ \forall p, q$, and matching points evenly spaced in the visible range. The number of beams $N_b = d/L_x$ was established via the pragmatic stability (scrambling) criterion discussed in Section IV-A.

this case, the choice of the *single* matching point is naturally more critical, and should be tailored to the reflection characteristics of the coating and/or to the incident field. Since no simple rule-of-thumb can be provided, we focused on the widely used normal-incidence (Leontovich) choice above, which provides a reasonable indication of the *average* performance.

For the same parameter configuration, Fig. 4 shows the copolar $(\Gamma_{\perp,\perp})$ and cross-polar $(\Gamma_{||,\perp})$ spectral reflection coefficients for perpendicular-polarization incidence (see (14)), computed using exact and approximate IBCs. The two reflection coefficients (note the different scales) exhibit sharp peaks and valleys around $k_x \approx \pm 0.25 k_0$ (i.e., spectral directions of about $\pm 15^\circ$ from the z-axis), which have been verified to arise from complex (leaky-wave) poles at $k_x \approx \pm(0.247 + i0.036)k_0$; this renders the chosen configuration particularly meaningful for testing the various asymptotic reductions developed in Sections III-B1 and III-B2. It is observed from Fig. 4 that the 2nd-order IBCs yield very accurate reflection coefficients. Moreover, although the corresponding impedance matching points were chosen within the visible range only (see Section IV-A and Appendix B), their effect extends into the invisible range. As before, 0th-order IBCs yield rather poor approximations for the reflection coefficients (not displayed), and fail completely in predicting the cross-polarization effects. Specifically, we found $\Gamma_{||,\perp} = 0$, and $\Gamma_{\perp,\perp}$ having unit magnitude in the visible range and exhibiting a pole singularity in the invisible range at $k_x \approx \pm 3.49 k_0$.

Concerning the reflected fields, we started with the most challenging case of $\theta_A = 15^\circ$, for which the interaction with the coating is maximum (see Fig. 4). The three reflected field components evaluated at a near-zone plane $(z = 10\lambda_0)$ are displayed in Fig. 5. The field has a dominant co-polar (y) component, but cross-polarization effects are not negligible. Note that for a perfectly conducting surface at $z = 0$ in the absence of the coating, and for the chosen parameter configuration, the observation plane would correspond to the focal plane. The presence of the coating modifies the reflected field pattern, but focusing effects can still be observed. For all three field components, the UMGB synthesis with second-order IBCs shows excellent agreement with the reference solution; here, any simplification in the beam asymptotics or in the IBCs would result in significant accuracy degradation. Specifically, SMGB synthesis with second-order IBCs gives only a reasonable prediction of the main peak(s), but is fairly inaccurate in the tails. Use of 0th-order IBCs yields again rather poor predictions, which are nonzero only for the copolar component; the approximated reflection coefficients tend to be rather flat, with pole singularities far away from the SP. As a consequence, no significant difference was observed between UMGB and SMGB syntheses, and only the computationally cheaper SMGB results are displayed [see Fig. 5(c) and (d)].

For a more quantitative accuracy assessment, Table I displays the maximum and average values of the normalized errors Δe_u for all three field components

$$\Delta e_u = \frac{|E_u^r - \mathcal{E}_u^r|}{\max|\mathcal{E}_u^r|}, \quad u = x, y, z \tag{40}$$

for the three syntheses in Fig. 5 and various incidence angles θ_A; $\mathcal{E}^r$ denotes the reference solution. It is observed that UMGB syntheses with second-order IBCs yield maximum errors $\lesssim -25$ dB and average errors $\lesssim -35$ dB, while SMGB syntheses are considerably less accurate. However, as the angle of incidence departs from the critical value of 15° (corresponding to the peaks in the reflection coefficients in Fig. 4), the effect of the leaky-wave poles becomes progressively less dominant. As a consequence, UMGB and SMGB syntheses (with second-order IBCs) tend to yield comparable accuracy.

TABLE I
PARAMETERS AS IN FIG. 5. MAXIMUM AND AVERAGE NORMALIZED ERRORS IN (40) FOR SMGB AND UMGB SYNTHESES, FOR ZEROTH- AND SECOND-ORDER IBCS AND FOR VARIOUS ANGLES OF INCIDENCE θ_A. ERRORS ARE COMPUTED IN A NEAR-ZONE $20\lambda_0 \times 20\lambda_0$ RECTANGULAR REGION WHEREIN THE FIELDS ARE SIGNIFICANTLY NONZERO, WITH $\lambda_0/2$ SAMPLING PERIOD

Beam synthesis and IBCs	θ_A	Normalized errors [dB]					
		$\Delta e_x^{(max)}$	$\Delta e_x^{(av)}$	$\Delta e_y^{(max)}$	$\Delta e_y^{(av)}$	$\Delta e_z^{(max)}$	$\Delta e_z^{(av)}$
UMGB, $N=2$	15^o	-30	-46	-27	-42	-27	-43
SMGB, $N=2$		-1	-11	-1	-11	-4	-14
SMGB, $N=0$		0	-11	0.5	-11	0	-13
UMGB, $N=2$	40^o	-32	-45	-35	-47	-32	-45
SMGB, $N=2$		-15	-25	-20	-30	-23	-34
SMGB, $N=0$		0	-14	-4	-18	0	-13
UMGB, $N=2$	60^o	-35	-48	-36	-50	-32	-47
SMGB, $N=2$		-24	-38	-30	-44	-30	-44
SMGB, $N=0$		0	-12	-6	-18	0	-11

The outcomes in Fig. 5 and Table I are indicative of the results obtained through several hundred numerical simulations involving different combinations of problem parameters. In general, reasonably accurate predictions (maximum errors $\lesssim -20$ dB and average errors $\lesssim -30$ dB) were observed for aperture field distributions with width $d > 5\lambda_0$ and distance $z_A > 2\lambda_0$, angles of incidence $|\theta_A| < 80°$, observation distances $z > 2\lambda_0$, and coatings with thickness $d_c < \lambda_0/\sqrt{\epsilon_r \mu_r}$ and chiral admittance $\gamma_c < 0.1\ \mathrm{ohm}^{-1}$. Parameter combinations falling outside these ranges need not to be doomed to failure a priori, but they require independent calibration.

2) Example 2: Four-Layer Complex Composite Coating and Abruptly Truncated Illumination: As a second challenging example, we have used a four-layer coating composed of: 1) a gyrotropic material, 2) a chiral material as in (38), 3) a dielectric, and 4) a uniaxial omega material. Referring to Fig. 1, the layers are arranged from bottom to top, with the bottom of layer 1 backed onto the perfectly conducting plane, and the top of layer 4 located at $z = 0$. The gyrotropic material is described by the following constitutive tensors:

$$\underline{\underline{\boldsymbol{\epsilon}}}_r = \epsilon_r \underline{\underline{\mathbf{I}}}, \quad \underline{\underline{\boldsymbol{\mu}}}_r = \begin{bmatrix} \mu_{ra} & -i\mu_{rb} & 0 \\ i\mu_{rb} & \mu_{ra} & 0 \\ 0 & 0 & \mu_{rz} \end{bmatrix}, \quad \underline{\underline{\boldsymbol{\xi}}} = \underline{\underline{\boldsymbol{\zeta}}} = 0 \quad (41)$$

which are typically used to describe biased ferrites [42]. Uniaxial omega media, introduced in [52], are characterized by the following constitutive tensors:

$$\underline{\underline{\boldsymbol{\epsilon}}}_r = \begin{bmatrix} \epsilon_{rt} & 0 & 0 \\ 0 & \epsilon_{rt} & 0 \\ 0 & 0 & \epsilon_{rz} \end{bmatrix}, \quad \underline{\underline{\boldsymbol{\mu}}}_r = \begin{bmatrix} \mu_{rt} & 0 & 0 \\ 0 & \mu_{rt} & 0 \\ 0 & 0 & \mu_{rz} \end{bmatrix},$$
$$\underline{\underline{\boldsymbol{\xi}}} = -\underline{\underline{\boldsymbol{\zeta}}}^T = \begin{bmatrix} 0 & i\Omega_l & 0 \\ -i\Omega_l & 0 & 0 \\ 0 & 0 & 0 \end{bmatrix} \quad (42)$$

where the superscript ^{T} denotes the transposed operator. Multilayer configurations like the one in this example have received attention as possible candidates for reduced-reflection coatings [6].

Numerical results for the near-zone reflected field are shown in Fig. 6, for the parameter configuration detailed in the figure caption. In these numerical experiments, we considered an *abruptly truncated* y-polarized linearly phased aperture field distribution as in (16) with $\mathbf{G}(x) = \mathbf{u}_y$, in order to emphasize edge-diffraction phenomena which were negligible in the previous example excitation. The spectral impedances and reflection coefficients (not shown for brevity) now exhibit a more regular (flatter) behavior than those of the previous example in Figs. 3 and 4. Consequently, as observed from Fig. 6, UMGB and SMGB syntheses with second-order IBCs were found to yield almost comparable accuracies. However, SMGB synthesis with zeroth-order IBCs still yield rather poor predictions. Specifically, maximum and average values of the normalized errors in (40) for UMGB syntheses were found to be $\Delta e^{(max)} \sim -24$ dB and $\Delta e^{(av)} \sim -37$ dB, respectively. For SMGB syntheses, we found $\Delta e^{(max)} \sim -14$ dB and $\Delta e^{(av)} \sim -30$ dB when using second-order IBCs, and $\Delta e^{(max)} \sim -6$ dB and $\Delta e^{(av)} \sim -17$ dB when using zeroth-order IBCs. Concerning the convergence of the beam syntheses, we found that in order to capture accurately the truncated-aperture-induced edge diffraction phenomena, a moderate increase in the number of beams ($N_b = 150$ versus $N_b = 50$ of the previous example) is required; this was already observed in [35] for the case of transmission through a single dielectric layer.

Due to the large number of parameters in this four-layer configuration, extensive calibration was indeed prohibitive. Nonetheless, outcomes from several hundred numerical simulations indicate that accurate syntheses ($\Delta e^{(max)} \lesssim -20$ dB and $\Delta e^{(av)} \lesssim -30$ dB) can generally be obtained providing the spectral reflection coefficients are accurately reproduced (within one percent error) via the approximate IBCs. Throughout, UMGB syntheses with second-order IBCs were found to provide the best accuracy, and therefore seem to be indicated for rather general applications. However, in particular applications featuring more "regular" reflection characteristics, SMGBs with second-order (and sometimes even zeroth-order) IBCs might be a computationally cheaper viable alternative.

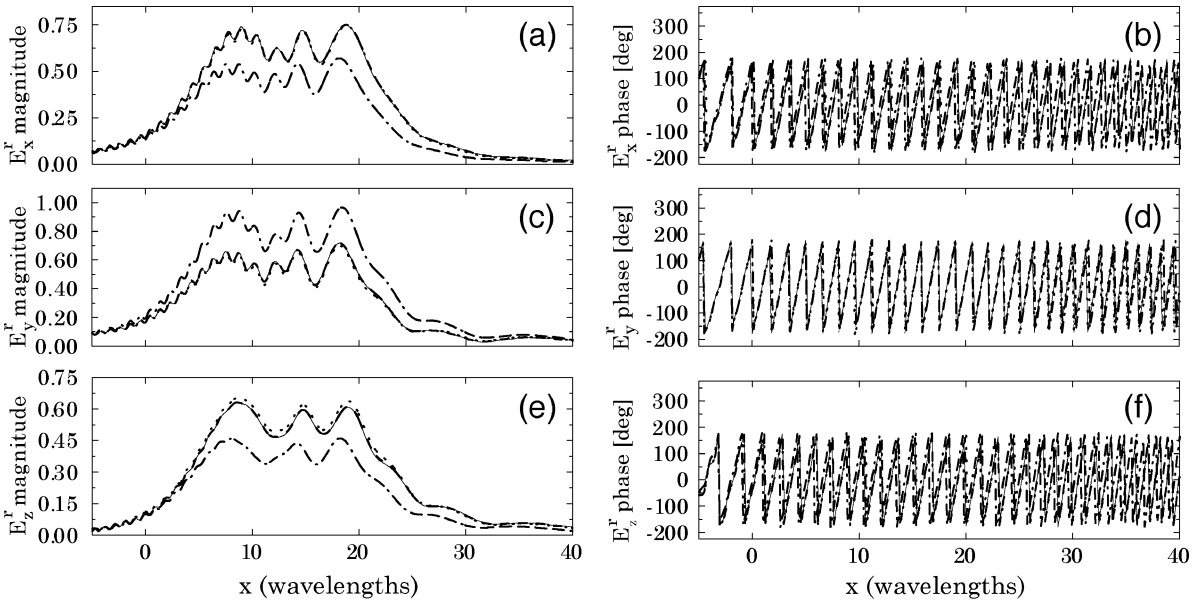

Fig. 6. Example 2: reflected fields. Four-layer coating and y-polarized abruptly truncated tilted aperture field distribution as in (16), with $\mathbf{G}(x) = \mathbf{u}_y$, $d = 20\lambda_0$, $z_A = 5\lambda_0$, $\theta_A = 40°$. Layer 1: gyrotropic material as in (41), with $\epsilon_r = 1.2$, $\mu_{ra} = 1.5$, $\mu_{rb} = 2.2$, $\mu_{rz} = 1.05$, $d_1 = 0.04\lambda_0$. Layer 2: chiral material as in (38), with $\epsilon_r = 4$, $\mu_r = 2$, $\gamma_c = 0.025\ \mathrm{ohm}^{-1}$, $d_2 = 0.05\lambda_0$. Layer 3: dielectric material with $\epsilon_r = 3 + i0.01$, $\mu_r = 1$, $d_3 = 0.035\lambda_0$. Layer 4: uniaxial omega material as in (42), with $\epsilon_{rt} = 3.5 + i0.02$, $\epsilon_{rz} = 2.5$, $\mu_{rt} = 3.5 + i0.01$, $\mu_{rz} = 4.4$, $\Omega_l = 0.05 + i0.01$, $d_4 = 0.04\lambda_0$. Layers are ordered from bottom to top, with the bottom of layer 1 backed onto the perfectly conducting plane, and the top of layer 4 placed at $z = 0$ (see Fig. 1). Near-zone reflected fields at $z = 10\lambda_0$. (a), (c), (e): E_x^r, E_y^r, E_z^r magnitude, respectively. (b), (d), (f): E_x^r, E_y^r, E_z^r phase, respectively. —— Reference solution (spectral integration); - - - NW-UMGB synthesis with 2nd-order IBCs ($N_b = d/L_x = 150$ beams); $\cdots\cdots$ NW-SMGB synthesis with second-order IBCs ($N_b = d/L_x = 150$ beams); $-\cdot-\cdot-\cdot-$ NW-SMGB synthesis with zeroth-order IBCs ($N_b = d/L_x = 150$ beams). All other simulation parameters as in Fig. 5.

C. Computational Features

Typical computing times, for a single-component field sample at a fixed observation point, are displayed in Table II. For the reference solution (spectral integration), computing times were found to depend almost linearly on the number of layers in the coating. This could be expected since the exact reflection coefficients (and thus the cascaded spectral impedances) need to be computed at each integration point. This is not the case for the beam syntheses based on the use of IBCs, for which the exact cascaded impedances are computed only once at the matching points (see Appendix B). Here, computing times depend in a linear fashion on the number of beams $N_b = d/L_x$. As could be expected, UMGB syntheses are computationally more demanding than SMGB, due the computation of additional terms that involve complex-argument error functions. Overall, beam syntheses with approximate IBCs were found to yield computing time savings ranging from one to two orders of magnitude as compared with the reference solution. Concerning comparison with conventional HF techniques (e.g., physical optics), we used as a benchmark the continuous limit (L_x, $b \to 0$) of our beam expansions which, as shown in Sections III-B1 and III-B2), reduces to Kirchhoff-type integral syntheses. Referring to the examples discussed in Section IV, we found that in order to achieve comparable accuracy, the numerical evaluation of the Kirchhoff integrals should be performed with a sampling rate ranging from 10 (for Example 1) to 20 (for Example 2) points per wavelengths. These estimates are consistent with our previous experience in applications of (Kirchhoff)-(physical-optics) formulations for other complex scattering scenarios [37], [41]. By comparison, Gabor-based beam discretization thus turns out to be computationally about 3–4 times cheaper; this better efficiency stems from the systematic utilization of *larger* "pixels" which are also *propagation-matched*.

TABLE II
TYPICAL COMPUTING TIMES PER SINGLE-COMPONENT REFLECTED FIELD SAMPLE AT A FIXED OBSERVATION POINT. ESTIMATES FOR THE REFERENCE SOLUTION (FOR TWO VALUES OF THE NUMBER OF LAYERS N_l) AND FOR THE VARIOUS BEAM SYNTHESES (FOR TWO VALUES OF THE NUMBER OF BEAMS $N_b = d/L_x$), BASED ON AVERAGE RUNNING TIMES ON A 550 MHz PC. ESTIMATES FOR UMGB SYNTHESES PERTAIN TO VALUES OF $M_{pq} = 6\ \forall p, q$ IN THE POLE-RESIDUE APPROXIMATIONS (31)

Synthesis		Time [secs]
Reference	$N_l = 1$	0.3
solution	$N_l = 4$	1.23
UMGB	$N_b = 50$	0.03
$(N = 2)$	$N_b = 150$	0.09
SMGB	$N_b = 50$	0.004
$(N = 2)$	$N_b = 150$	0.012
SMGB	$N_b = 50$	0.03
$(N = 0)$	$N_b = 150$	0.09

V. CONCLUSION

A Gabor-based narrow-waisted (NW) Gaussian beam (GB) algorithm has been utilized here to determine the 2-D time-harmonic scattering of finite-aperture-generated EM fields by planar conducting surfaces coated with multiple layers of homogeneous bi-anisotropic media described by higher-order impedance boundary conditions (HOIBCs). To the best of our

knowledge, large-aperture localized (including focusing and abruptly truncated) illuminations have not been considered previously in the HOIBC literature, nor has the combined use of HOIBCs and Gabor-based NW-GB algorithms.

Various beam syntheses based on zeroth- and second-order IBCs, have been derived via conventional (nonuniform) and modified (uniform) complex-source-point paraxial asymptotics, and have been validated and calibrated against a rigorously based numerical brute-force-evaluated reference solution. Numerical results for the reflected fields, pertaining to complex multi-layer coatings under focusing and abruptly truncated illuminations, indicate that the proposed beam algorithm is able to furnish accurate and computationally efficient solutions for this complex propagation environment, over a range of calibrated combinations of the problem parameters. Performance comparisons have also been made with direct numerical evaluation of Kirchhoff-type integral representations.

One of the potential uses of the NW-GB algorithm is as an efficient solver for wave scattering problems arising in analysis and control of radar signatures. In this connection, we are currently working on extending the present formulation to accommodate *smooth nonplanar* objects and *slowly varying* transverse inhomogeneities. In such scenarios, the exciting aperture field distribution in Fig. 1 would be replaced by an equivalent physical-optics-like current distribution placed onto the illuminated portion of the scatterer, and a *locally planar* approximation would be invoked to apply *adiabatically* the formulations derived in the present paper. Other worthwhile extensions include fully 3-D scenarios, and pulsed excitations.

APPENDIX A
SYMMETRY RELATIONS FOR ZEROTH- AND SECOND-ORDER IMPEDANCE BOUNDARY CONDITIONS

As mentioned in Section II-B, the assumed rotational symmetry in the coating yields a number of constraints relating the coefficients $c_{\mu,\nu}$ in the HOIBCs (4). One finds [22, Appendix B]

$$c_{\mu,\nu} = 0, \quad \text{for } \nu \text{ odd}, \quad \mu = 1, \ldots, 8, \tag{43}$$

$$c_{1,0} = c_{4,0} = 1, \quad c_{2,0} = c_{3,0} = 0,$$

$$c_{7,0} = -c_{6,0}, \quad c_{8,0} = c_{5,0}. \tag{44}$$

It follows that the number of independent coefficients to be determined is two for zeroth-order $(N = 0)$ IBCs, and ten for second-order $(N = 2)$ IBCs.

APPENDIX B
HOIBC DERIVATION

In [22], a systematic approach was introduced for deriving HOIBCs for planar and curved coatings consisting of single layers of homogeneous dielectric or chiral media. This approach has subsequently been extended in [29], [31], [32] to accommodate arbitrary combinations of inhomogeneous (in the direction normal to the boundary) dielectric layers and homogeneous bianisotropic media, The approach is based on the derivation of *exact* spectral domain IBCs which, for a large class of materials, can be obtained analytically. For the case of bianisotropic multilayers, the exact IBCs are computed in each layer via decomposition of the fields in terms of *characteristic waves*, and are subsequently cascaded (see [31, Section 2.1] for details). Such exact spectral IBCs are then approximated in terms of finite-order rational functions of the spectral variable(s) (in our case k_x) via a point-matching procedure (see [22, Section 3.1.2], [31, Appendix B] for details), yielding the approximate relations in (7) or their spatial-domain counterpart in (4). In this connection, symmetry considerations are exploited to reduce the number of coefficients $c_{\mu,\nu}$ to be determined via point-matching (see Appendix A). For zeroth-order (Leontovich-type) IBCs, the two unknown coefficients (see Appendix A) are usually determined by matching the exact and approximate impedances at normal incidence $(k_x = 0)$. For second-order IBCs, three matching points are used to compute the ten unknown coefficients (see Appendix A). Typical values are $k_x = 0$, $k_0/2$, and k_0, so as to span the entire visible range. Extension of these canonical HOIBCs to accommodate *smooth nonplanar* objects and *slowly varying* transverse inhomogeneities can be pursued via consistent use of locally planar [22], [31] or locally cylindrical [22], [32] approximations, which result in position-dependent $c_{\mu,\nu}$ coefficients. Abrupt variations or discontinuities in the coating parameters can also be accommodated in principle, at the expense of enforcing additional constraints [53]. Moreover, for the assumed rotationally symmetric coatings, extension to the full 3-D case follows trivially via simple symmetry considerations [22].

ACKNOWLEDGMENT

The authors would like to express their appreciation to an anonymous reviewer for the careful reading of the paper, with helpful comments.

REFERENCES

[1] N. Engheta and D. L. Jaggard, "Electromagnetic chirality and its applications," *IEEE Antennas Propagat. Soc. Newsletter*, vol. 30, pp. 6–12, Oct. 1988.

[2] R. A. Shelby, D. D. R. Smith, and S. Schultz, "Experimental verification of a negative index of refraction," *Science*, vol. 292, no. 5514, pp. 77–79, Apr. 2001.

[3] R. W. Ziolkowski and N. Engheta, Guest Editors, "Special Issue on Metamaterials," *IEEE Trans. Antennas Propagat.*, vol. 51, Oct. 2003.

[4] V. K. Varadan, V. V. Varadan, and A. Lakhtakia, "On the possibility of designing anti-reflection coatings using chiral composites," *J. Wave-Material Interaction*, vol. 2, no. 1, pp. 71–81, Jan. 1987.

[5] M. Norgren and S. He, "On the possibility of reflectionless coating of a homogeneous bianisotropic layer on a perfect conductor," *Electromagn.*, vol. 17, no. 4, pp. 295–307, July–Aug. 1997.

[6] M. Norgren, "Optimal design using stratified bianisotropic media: application to anti-reflection coatings," *J. Electromagn. Waves Appls.*, vol. 12, pp. 939–959, 1998.

[7] F. Olyslager and I. V. Lindell, "Electromagnetics and exotic media: a quest for the holy grail," *IEEE Antennas Propagat. Mag.*, vol. 44, pp. 48–58, Apr. 2002.

[8] M. S. Kluskens and E. H. Newman, "Scattering by a multilayer chiral cylinder," *IEEE Trans. Antennas Propagat.*, vol. 39, pp. 91–96, Jan. 1991.

[9] R. D. Graglia, P. L. E. Uslenghi, and C. L. Yu, "Electromagnetic oblique scattering by a cylinder coated with chiral layers and anisotropic jump-immittance sheets," *J. Electromagn. Waves Appls.*, vol. 6, no. 5/6, pp. 695–719, 1992.

[10] P. L. Huddleston, L. N. Medgyesi-Mitschang, and J. M. Putnam, "Combined field integral equation formulation for scattering by dielectrically coated conducting bodies," *IEEE Trans. Antennas Propagat.*, vol. AP-34, pp. 510–520, Apr. 1986.

[11] J. M. Jin and V. Liepa, "Application of hybrid finite element to electromagnetic scattering from coated cylinders," *IEEE Trans. Antennas Propagat.*, vol. AP-36, pp. 50–54, Jan. 1988.
[12] M. A. Leontovich, *Investigations on Radiowave Propagation*. Moscow: Academy of Sciences, 1948, pt. II.
[13] S. N. Karp and F. C. Karal Jr., "Generalized impedance boundary conditions with application to surface wave structures," in *Electromagnetic Theory*. New York: Pergamon, 1965, pt. I, pp. 479–483.
[14] A. L. Weinstein, *The Theory of Diffraction and the Factorization Method*. Boulder, CO: Golem, 1969.
[15] N. G. Alexopoulos and G. A. Tadler, "Accuracy of the Leontovich boundary condition for continuous and discontinuous surface impedance," *J. Appl. Phys.*, vol. 46, no. 8, pp. 3326–3332, Aug. 1975.
[16] T. B. A. Senior and J. L. Volakis, "Derivation and application of a class of generalized impedance boundary conditions," *IEEE Trans. Antennas Propagat.*, vol. AP-37, pp. 1566–1572, Dec. 1989.
[17] R. G. Rojas and Z. Al-hekail, "Generalized impedance/resistive boundary conditions for electromagnetic scattering problems," *Radio Sci.*, vol. 24, no. 1, pp. 1–12, Jan.–Feb. 1989.
[18] M. Idemen, "Universal boundary conditions of the electromagnetic fields," *J. Phys. Soc. Jpn.*, vol. 59, no. 1, pp. 71–80, Jan. 1990.
[19] K. Barkeshli and J. L. Volakis, "TE scattering by a one-dimensional groove in a ground-plane using higher-order impedance boundary conditions," *IEEE Trans. Antennas Propagat.*, vol. 38, pp. 1421–1428, Sept. 1990.
[20] T. B. A. Senior and J. L. Volakis, "Generalized impedance boundary conditions in scattering," *Proc. IEEE*, vol. 79, no. 10, pp. 1413–1420, Oct. 1991.
[21] D. J. Hoppe and Y. Rahmat-Samii, "Scattering by superquadric dielectric-coated cylinder using higher order impedance boundary conditions," *IEEE Trans. Antennas Propagat.*, vol. 40, pp. 1513–1523, Dec. 1992.
[22] ——, *Impedance Boundary Conditions in Electromagnetics*. Washington, DC: Taylor & Francis, 1995.
[23] T. B. A. Senior and J. L. Volakis, *Approximate Boundary Conditions in Electromagnetics*. Stevenage, U.K.: IEE Press, 1995.
[24] R. Cicchetti, "A class of exact and higher order surface boundary conditions for layered structures," *IEEE Trans. Antennas Propagat.*, vol. 44, pp. 249–259, Feb. 1996.
[25] H. Ammari and S. He, "Generalized effective impedance boundary conditions for an inhomogeneous thin layer in electromagnetic scattering," *J. Electromagnetic Waves Appls.*, vol. 11, no. 9, pp. 121–1197, Sep. 1997.
[26] S. A. Tretyakov, "Generalized impedance boundary conditions for isotropic multilayers," *Microwave Opt. Technol. Lett.*, vol. 17, no. 4, pp. 262–265, Mar. 1998.
[27] H. Ammari and S. He, "Effective impedance boundary conditions for an inhomogeneous thin layer on a curved metallic surface," *IEEE Trans. Antennas Propagat.*, vol. 46, pp. 710–715, May 1998.
[28] D. Y. Khaliullin and S. A. Tretyakov, "Reflection and transmission coefficients for thin bianisotropic layers," *Proc. Inst. Elec. Eng. Microwave Antennas Propagat.*, vol. 145, no. 2, pp. 163–168, Apr. 1998.
[29] V. Galdi and I. M. Pinto, "Higher-order impedance boundary conditions for metal-backed inhomogeneous dielectric layers," *Microwave Opt. Technol. Lett.*, vol. 22, no. 4, pp. 249–254, Aug. 1999.
[30] M. Norgren and S. He, "Effective boundary conditions for a 2D inhomogeneous nonlinear thin layer coated on a metallic surface," in *Progress in Electromagnetics Research*, J. A. Kong, Ed. Boston, MA: EMW, Nov. 1999, vol. 23, pp. 301–315.
[31] V. Galdi and I. M. Pinto, "Derivation of higher-order impedance boundary conditions for stratified coatings composed of inhomogeneous-dielectric and homogeneous-bianisotropic layers," *Radio Science*, vol. 35, no. 2, pp. 287–303, Mar.–Apr. 2000.
[32] ——, "SDRA approach for higher-order impedance boundary conditions for complex multi-layer coatings on curved conducting bodies," in *Progress in Electromagnetics Research*, J. A. Kong, Ed. Boston, MA: EMW, Dec. 1999, vol. 24, pp. 311–335.
[33] O. Marceaux and B. Stupfel, "High-order impedance boundary conditions for multilayer coated 3-D objects," *IEEE Trans. Antennas Propagat.*, vol. 48, pp. 429–436, Mar. 2000.
[34] J. J. Maciel and L. B. Felsen, "Systematic study of fields due to extended apertures by Gaussian beam discretization," *IEEE Trans. Antennas Propagat.*, vol. 37, pp. 884–892, July 1989.
[35] ——, "Gaussian beam analysis of propagation from an extended aperture distribution through dielectric layers: Part I—plane layer," *IEEE Trans. Antennas Propagat.*, vol. 38, pp. 1607–1617, Oct. 1990.
[36] ——, "Gaussian beam analysis of propagation from an extended aperture distribution through dielectric layers: Part II—circular cylindrical layer," *IEEE Trans. Antennas Propagat.*, vol. 38, pp. 1618–1624, Oct. 1990.
[37] V. Galdi, L. B. Felsen, and D. A. Castañon, "Quasiray Gaussian beam algorithm for time-harmonic two-dimensional scattering by moderately rough interfaces," *IEEE Trans. Antennas Propagat.*, vol. 49, pp. 1305–1314, Sept. 2001.
[38] ——, "Narrow-waisted Gaussian beam discretization for two-dimensional time-dependent radiation from large apertures," *IEEE Trans. Antennas Propagat.*, vol. 49, pp. 1322–1332, Sept. 2001.
[39] ——, "Quasiray Gaussian beam algorithm for short-pulse two-dimensional scattering by moderately rough dielectric interfaces," *IEEE Trans. Antennas Propagat.*, vol. 51, pp. 171–183, Feb. 2003.
[40] V. Galdi and L. B. Felsen, "Two-dimensional pulsed propagation from extended aperture field distributions through a planar dielectric layer via quasiray Gaussian beams," *IEEE Trans. Antennas and Propagat.*, vol. 51, pp. 1549–1558, July 2003.
[41] L. B. Felsen and V. Galdi, "Aperture-radiated electromagnetic field synthesis in complex environments via narrow-waisted Gabor-discretized Gaussian beams," *AEÜ Int. J. Electronics Commun.*, vol. 57, no. 2, pp. 84–99, Mar. 2003.
[42] J. A. Kong, *Theory of Electromagnetic Waves*. New York: Wiley, 1975.
[43] T. B. Hansen and A. D. Yaghjian, *Plane-Wave Theory of Time-Domain Fields: Near-Field Scanning Applications*. Piscataway, NJ: IEEE, 1999.
[44] M. J. Bastiaans, "Gabor's expansion of a signal into Gaussian elementary signals," *Proc. IEEE*, vol. 68, pp. 538–539, 1980.
[45] L. B. Felsen and N. Marcuvitz, *Radiation and Scattering of Waves*. Englewood Cliffs, NJ: Prentice Hall, 1973.
[46] E. K. Miller and G. J. Burke, Some applications of model-based parameter estimation in computational electromagnetics, in Modern Antenna Design Using Computer and Measurements: Application to Antenna Problem of Military Interest, vol. 65, ser. AGARD Lecture Series, pp. 4.1–4.26, 1989.
[47] V. I. Kukulin, V. M. Krasnopol'sky, and J. Horácek, *Theory of Resonances. Principles and Applications*. Praha: Academia, 1989.
[48] M. Abramowitz and I. A. Stegun, *Handbook of Mathematical Functions*. New York: Dover, 1964.
[49] H. D. Cheung and E. V. Jull, "Two-dimensional diffraction by half-planes and wide slits near radiating apertures," *IEEE Trans. Antennas Propagat.*, vol. 47, pp. 1669–1676, Nov. 1999.
[50] W. H. Press, S. A. Teukolsky, W. T. Vetterling, and B. P. Flannery, *Numerical Recipes in C: The Art of Scientific Computing*, 2nd ed. Cambridge, U.K.: Cambridge Univ. Press, 1992.
[51] H. E. Salzer, "Formulas for calculating the error function of a complex variable," *Math. Tables Aids Comp.*, vol. 5, pp. 67–70, 1951.
[52] N. Engheta and M. M. I. Saadoun, "A reciprocal phase shifter using novel pseudochiral or Ω medium," *Microwave Opt. Technol. Lett.*, vol. 5, no. 4, pp. 184–187, Apr. 1992.
[53] T. B. A. Senior, "Generalized impedance boundary conditions and the question of uniqueness," *Radio Science*, vol. 27, no. 6, pp. 929–934, Nov.–Dec. 1992.

Vincenzo Galdi (M'98) was born in Salerno, Italy, on July 28, 1970. He received the Laurea degree (*summa cum laude*) in electrical engineering and the Ph.D. degree in applied electromagnetics from the University of Salerno, Italy, in 1995 and 1999, respectively.

From April to December 1997, he held a visiting position in the Radio Frequency Division of the European Space Research & Technology Centre (ESTEC-ESA), Noordwijk, The Netherlands. From September 1999 to August 2002, he held a Research Associate position in the Department of Electrical and Computer Engineering at Boston University, Boston, MA. In September 2002, he was appointed Associate Professor of Electromagnetics, and joined the Department of Engineering at the University of Sannio, Benevento, Italy, where he is currently working. His research interests include analytical and numerical techniques for wave propagation in complex environments, electromagnetic chaos, and inverse scattering.

Dr. Galdi is the recipient of a 2001 International Union of Radio Science (URSI) "Young Scientist Award." He is a Member of Sigma Xi.

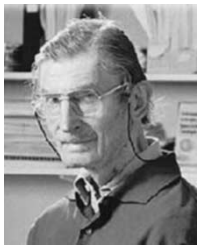

Leopold B. Felsen (S'47–M'54–SM'55–F'62–LF'90) was born in Munich, Germany, on May 7, 1924. He received the B.E.E., M.E.E, and D.E.E. degrees from the Polytechnic Institute of Brooklyn, Brooklyn, NY, in 1948, 1950, and 1952, respectively.

He emigrated to the United States in 1939 and served in the U.S. Army from 1943 to 1946. After 1952, he remained with the Polytechnic (now Polytechnic University), gaining the position of University Professor in 1978. From 1974 to 1978, he was Dean of Engineering. In 1994, he resigned from the full-time Polytechnic faculty and was granted the status of University Professor Emeritus. He is now Professor of Aerospace and Mechanical Engineering and Professor of Electrical and Computer Engineering at Boston University, Boston, MA (part-time). He is the author or coauthor of over 350 papers and of several books, including the classic *Radiation and Scattering of Waves* (Piscataway, NJ: IEEE Press, 1994). He is an associate editor of several professional journals and was an editor of the Wave Phenomena Series (New York: Springer-Verlag). His research interests encompass wave propagation and diffraction in complex environments and in various disciplines, high-frequency asymptotic and short-pulse techniques, and phase-space methods with an emphasis on wave-oriented data processing and imaging.

Dr. Felsen is a Member of Sigma Xi and a Fellow of the Optical Society of America (OSA) and the Acoustical Society of America. He has held named Visiting Professorships and Fellowships at universities in the United States and abroad, including the Guggenheim in 1973 and the Humboldt Foundation Senior Scientist Award in 1981. In 1974, he was an IEEE/APS (Antennas and Propagation Society) Distinguished Lecturer. His Poet's Corner appears sporadically in the IEEE/APS Magazine. He received the IEEE/APS Best Paper Award in 1969, and was coauthor for 1974 and 1981; he was contributing author to papers selected for the R.W.P. King Award for 1984, 1986, and 2000. Moreover, he received the Balthasar van der Pol Gold Medal from the International Union of Radio Science (URSI) in 1975, an honorary doctorate from the Technical University of Denmark in 1979, the IEEE Heinrich Hertz Gold Medal for 1991, the APS Distinguished Achievement Award for 1998, the IEEE Third Millenium Medal in 2000 (nomination by APS), an honorary Laurea degree from the University of Sannio in Benevento, Italy, in 2003, the IEEE Electromagnetics Award for 2003, an honorary doctorate from the Technical University of Munich, Germany, in 2004, three Distinguished Faculty Alumnus Awards from Polytechnic University, and an IEEE Centennial Medal in 1984. In 1977, he was elected to the National Academy of Engineering. He has served on the APS Administrative Committee from 1963 to 1966, and was Vice Chairman and Chairman for both the United States (1966–1973) and the International (1978–1984) URSI Commission B.

Innocenzo M. Pinto (M'99) was born and educated in Italy. Winner of national competitions, he was appointed Assistant Professor of Electromagnetics in 1983, Associate Professor in 1987, and Full Professor in 1990. He has been a faculty member in the Universities of Naples, Salerno (where he founded and Chaired the Ph.D. program in Information Engineering from 1993 to 2001), Catania, and Sannio at Benevento, where he is currently the Dean of the Information Engineering Curricula Committee. He has visited several research institutions as an Invited Lecturer, including CERN, KEK, and NIST (former NBS). In 1998, he was an EU Senior Visiting Scientist at the National Astronomical Observatory, Tokyo, Japan, in connection with TAMA300 experiment. He has authored or coauthored more than 100 technical papers in peer-reviewed international journals. His research interests span from electrophysics to gravitational wave experiments.

Dr. Pinto is a Member of the American Physical Society.